Transactions on Engineering and Computing Sciences - Vol. 13, No. 06
Publication Date: December 27, 2025
DOI:10.14738/tmlai.1306.19748.
Sorescu, M., Kelly, J., & Aitken, J. (2025). Optical Absorption Bands in the Milled Gallium Oxide-hematite Nanoparticles System. *Transactions on Engineering and Computing Sciences*, 13(06). 299-308.

Optical Absorption Bands in the Milled Gallium Oxide-hematite Nanoparticles System

Monica Sorescu
School of Science and Engineering,
Duquesne University, Pittsburgh, PA, United States

Jordan Kelly
School of Science and Engineering,
Duquesne University, Pittsburgh, PA, United States

Jennifer Aitken
School of Science and Engineering,
Duquesne University, Pittsburgh, PA, United States

ABSTRACT

Nanoparticles of the gallium oxide-hematite mixed-oxide system were synthesized by mechanochemical activation using high-energy ball milling for durations of 0, 2, 4, 8, and 12 hours. Optical diffuse reflectance spectroscopy (ODRS) measurements were performed across the full UV-VIS-NIR range. Optical absorption bands in the spectra of hematite and gallium oxide nanoparticles were identified. Hematite (a-Fe_2O_3) exhibits a strong absorption band in the visible range (~2.2 eV), while other prominent absorption bands are located at ~3.1-3.2 eV and ~5.3-5.8 eV. These features arise from the electronic structure of the iron ions and the crystal lattice, with antiferromagnetic interactions in certain structural configurations enhancing the intensity of the absorption bands. b-Ga_2O_3 has an intrinsic bandgap of approximately 4.8 eV, rendering it transparent throughout the visible and into the deep-UV region. Free electrons in doped Ga_2O_3 can absorb light from the IR to UV via transitions between conduction bands, including a direct optical transition that occurs at approximately 3.55 eV (349 nm). The optical absorption properties of the gallium oxide-hematite system were found to depend on the milling processing parameters.

Keywords: Hematite, Gallium oxide, Optical diffuse reflectance spectroscopy, Optical absorption bands, Nanoparticles.

INTRODUCTION

Hematite (a-Fe_2O_3) has been the focus of various theoretical and experimental studies owing to its applications as a magnetic, semiconducting, and catalytic material. Doping hematite with various transition metal and rare earth elements has been shown to enhance its electrochemical and photocatalytic properties [1-6].

Gallium oxide (Ga_2O_3) is a paramagnetic compound that can be used to functionalize hematite with prospective applications in sensing, catalysis and flexible electronics. In particular, gallium ion Ga^{3+} was found to exhibit intriguing properties when introduced in several systems. A

comprehensive density functional theory (DFT) investigation of defects in gallium oxide was performed in [7]. Ambient-condition strategy for rapid mass production of crystalline gallium oxide nanoarchitectures toward device applications was developed in [8]. Bandgap engineering of gallium oxides by crystalline disorder was accomplished in [9] for applications in high-power and radio frequency electronics and deep-ultraviolet optoelectronics. Deep UV transparent thin films were realized in [10] through degenerately doped wide-bandgap gallium oxide. Defect-assisted photocatalytic activity of glass-embedded gallium oxide nanocrystals was achieved in [11]. The electronic structure and chemical bonding in transition-metal-mixed gallium oxide compounds was studied in [12] for optoelectronic and photovoltaic applications. Gallium oxide nanoparticles were prepared in [13] through solid state route for efficient photovoltaic overall water splitting. High-rate growth of gallium oxide films by plasma-enhanced thermal oxidation for solar-blind photodetectors was achieved in [14]. The kinetics of structural transformations during mechanical high energy milling of hematite and gallium was investigated in [15] in order to reveal the mechanism of the process. Mthe olten Ga spread over freshly prepared surfaces during the milling process and was incorporated into the hematite intermediate oxides structures. Optical constants of titanium-doped gallium oxide thin films were determined in [16]. Oxygen sensors based on gallium oxide thin films with addition of chromium were constructed in [17]. Synthesis and characterization of gallium oxide were performed in [18] in strong reducing growth ambient by chemical vapor deposition. Tunable properties - including wide spectral selectivity, a red-shifted bandgap, and electrocatalytic behavior - of an iron-doped gallium oxide model system were reported in [19]. The monoclinic crystal structure of *b*-Ga_2O_3 resulted in optical anisotropy under incident light with different polarization states, as discussed in [20]. It was found that free electrons in n-doped b-Ga_2O_3 absorb light from the IR to the UV wavelength range via intra- and inter-conduction band optical transitions. Chemical and photochemical processes described in [21] at semiconductor surfaces were highly influenced by the size of the bandgap and the ability to control the bandgap by the particle size of nanomaterials. Luminescence properties of gallium oxide powders obtained from intra-bandgap photoluminescence (PL) measurements were reported in [22]. The influence of growth time on the structural, optical, and optoelectronic properties of b-Ga_2O_3 films produced on Si substrates by the chemical vapor deposition method was studied in [23]. Enhanced red-shifting in the optical bandgap of b-Ga_2O_3 films was reported in [24].

Recently, the ball milling technique has proven to be key for obtaining garnet-graphene nanocomposites [25] and has been crucial in determining the formation of the skyrmion phase in the Fe-Co-Si system [26]. Moreover, mechanochemical activation was used to synthesize mixed-oxide nanostructures of the type xGd_2O_3-(1-x)a-Fe_2O_3 [27] and xDy_2O_3-(1-x)a-Fe_2O_3 [28] with the formation of solid solutions in the systems.

In the present study, we aim to shed light on the optical properties of the xGa_2O_3-(1-x)a-Fe_2O_3 system with molar concentration x=0.5, obtained by mechanochemical activation at different ball milling times. Our investigations are focused on optical diffuse reflectance spectroscopy (ODRS) of the gallium oxide-hematite nanoparticles over the entire UV-VIS-NIR range. Optical absorption bands in hematite and gallium oxide nanostructures were identified.

MATERIALS AND METHODS

Nanoparticles of xGa_2O_3-(1-x)a-Fe_2O_3 (x=0.5) were obtained by mechanochemical activation of precursor powders of hematite and gallium oxide (Alfa Aesar), with particle sizes on the order of several tens of nanometers. The powders were mixed manually using a mortar and pestle and introduced in a SPEX 8000 mixer mill. They were milled for time periods of 0, 2, 4, 8, and 12 hours. The powder to ball ratio was 1:5.

Optical diffuse reflectance spectroscopy (ODRS) was performed on the milled gallium oxide-hematite nanoparticles over the entire UV-VIS-NIR range. Data from 2500 to 200 nm were collected with a Varian Cary 5000 UV-VIS-NIR spectrophotometer coupled with a diffused reflectance accessory at a rate of 600 nm min^{-1}. The 100% reflectance standard was $BaSO_4$ (Fisher Scientific, 99.92%). The sample was ground and pressed on top of the reference that was preloaded in the sample cup. Reflectance data were converted to absorption by employing the Kubelka-Munk equation. Optical absorption bands in the gallium oxide-hematite nanostructures were identified. The spectra were computer analyzed and plotted using SigmaPlot. User-defined transforms were utilized for the power variables.

RESULTS

To characterize the optical property changes induced by mechanochemical activation in the gallium oxide-hematite milled system, optical diffuse reflectance spectroscopy (ODRS) measurements were undertaken in the present study. Figure 1 (a) shows the optical absorption spectra of the gallium oxide-hematite equimolar mixture as a function of energy over the UV-VIS-NIR spectral range for all milling times employed. For the starting material, hematite has a bandgap of 1.9-2.2 eV in the visible region, while gallium oxide exhibits absorption bands primarily in the UV region. For the ball-milled materials, the absorbance is considerably enhanced and broadened, an effect we believe to result from the substitution of Ga ions for Fe.

According to Tauc plots, the dependance of $(aE)^2$ as a function of energy (eV) yields the bandgap of the compound. The exponent of 2 was chosen because the 2.2 eV transition in hematite is indirect. Indeed, it can be observed in Figure 1 (b) that the intercepts give a value of ~2.1 eV for the band gap. This value is independent of the milling time employed. It can be seen in this figure that there is no absorption below 2.1 eV for all milling times, while above the bangap there is a broad absorption that depends on the milling time employed. These results show that the gallium oxide-hematite mixed-oxide nanostructures have semiconductor properties.

DISCUSSION

Hematite (a-Fe_2O_3) has prominent absorption bands around 2.2 eV, 3.1-3.2 eV and 5.3-5.8 eV. Gallium oxide (Ga_2O_3) shows absorption features that depend on its phase and doping, with a wide bandgap (4.8 eV for b-Ga_2O_3) and additional absorption from defect-related transitions and free carriers in the visible to UV range. Hematite (a-Fe_2O_3) has a significant absorption band in the visible range (~2.2 eV). Another prominent absorption band is located at ~3.1-3.2 eV. A higher energy absorption band is present at ~5.3-5.8 eV. These bands are related to the electronic structure of the iron ions and the crystal lattice, with antiferromagnetic interactions in certain structures enhancing the intensity of the absorption bands.

The intrinsic bandgap for b-Ga_2O_3 is approximately 4.8 eV, meaning it is transparent to visible light into deep UV. Free electrons in doped Ga_2O_3 can absorb light from the IR to UV via transitions between conduction bands. A direct optical transition occurs between conduction bands at approximately 3.55 eV (349 nm). Doping introduces defect levels that cause additional absorption. For example, Fe-doped Ga_2O_3 shows transitions at 1.2 eV, 2.3 eV, and 3.0 eV, while Mg-doped Ga_2O_3 can show absorption at 1.6 eV. While this is about absorption, related emission bands have been observed at approximately 3.8 eV (UV), 3.0 eV (blue), and 2.1 eV (red).

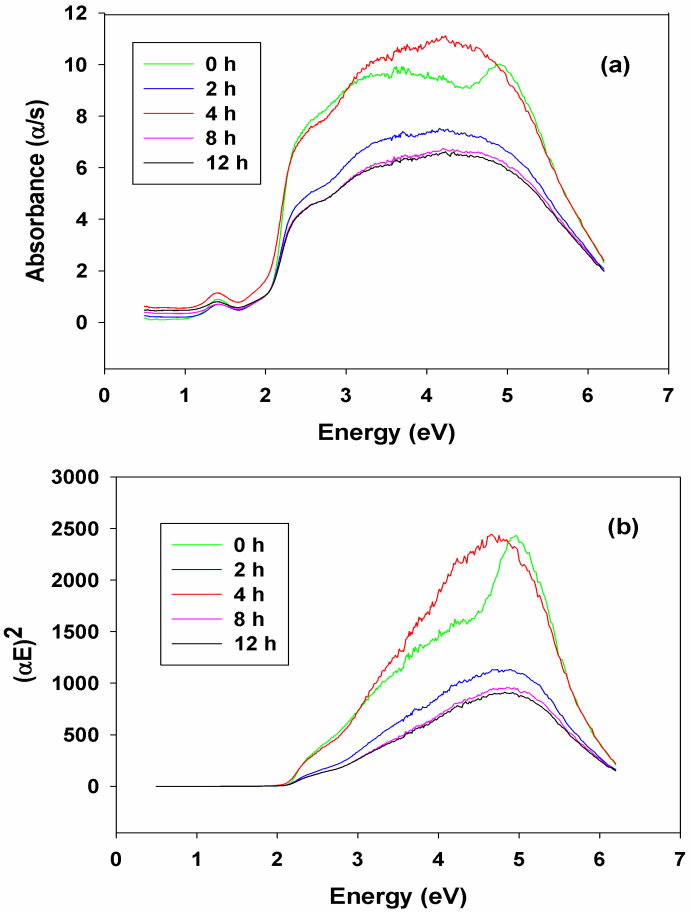

Figure 1: Optical absorption spectra of the gallium oxide-hematite nanoparticles.

Quantum confinement in hematite (α-Fe_2O_3) nanostructures occurs in nanoparticles (<10 nm), in which the bandgap can widen slightly blue-shifting absorption toward shorter wavelengths. High surface-to-volume ratio introduces defect states that enhance sub-bandgap absorption, often improving photocatalytic activity. Orientation and crystallinity strongly affect absorption. For example, epitaxial films can suppress unwanted recombination, sharpening absorption edges, while mechanical milling introduces strain and defects, which broaden absorption bands and can create mid-gap states that extend absorption into the visible. Doping (e.g., Ti, Sn, Si) alters Fe^{3+} electronic environment, shifting charge-transfer bands and improving conductivity for photoelectrochemical applications.

Bandgap tuning in gallium oxide (b-Ga_2O_3) nanostructures, such as nanowires and nanosheets can slightly modify the bandgap (~4.7–5.2 eV), shifting the UV absorption edge. Oxygen vacancies or dopants (Sn, Si, Ge) introduce donor states, leading to additional absorption features in the visible/near-IR. Orientation dependence is pronounced: monoclinic symmetry means absorption anisotropy can be engineered by film growth direction. Ball milling creates amorphous or nanocrystalline Ga_2O_3 with broadened absorption edges, useful for tailoring transparency and defect-related absorption. Controlled defect absorption enables UV photodetectors with tunable cutoff wavelengths, and transparent electronics that remain visible-light transparent but UV-sensitive. Comparative insights into the features of hematite and gallium oxide nanostructures are listed in Table 1.

Table 1: Comparative Insights

Feature	Hematite Nanostructures	Gallium Oxide Nanostructures
Bandgap shift	Slight widening (blue shift)	Slight widening, anisotropy effects
Defect/strain effects	Mid-gap states enhance visible absorption	Oxygen vacancies add donor states
Thin film orientation	Affects recombination and absorption edge	Strong anisotropy in absorption
Doping impact	Improves conductivity, shifts charge transfer	Introduces donor levels, tunes UV cutoff
Industrial applications	Solar water splitting, photocatalysis	UV photodetectors, transparent power electronics

To summarize, nanostructuring broadens and shifts absorption bands by introducing quantum confinement, defects, and orientation effects. Hematite benefits by extending visible absorption for solar energy, while gallium oxide gains tunable UV sensitivity without losing visible transparency.

Tunable properties in terms of wide spectral selectivity, red-shifted bandgap, and electrocatalytic behavior of iron-doped gallium oxide model system were reported in [29]. X-ray diffraction (XRD) studies of sintered $Ga_{2-x}Fe_xO_3$ (GFO) ($0.0 \le x \le 0.3$) compounds provide evidence for the Fe^{3+} substitution at the Ga^{3+} site without any secondary phase formation. Rietveld refinement of XRD patterns reveals that the GFO compounds crystallize in monoclinic crystal symmetry with a C2/m space group. The electronic structure of the GFO compounds probed using X-ray photoelectron spectroscopy data reveals that at lower concentrations, Fe exhibits mixed chemical valence states (Fe^{3+}, Fe^{2+}), whereas single chemical valence state (Fe^{3+}) is evident for higher Fe content ($x = 0.20–0.30$). The optical absorption spectra reveal a significant red shift in the optical bandgap with Fe doping. The origin of the significant red shift even at low concentrations of Fe ($x = 0.05$) is attributed to the strong sp−d exchange interaction originating from the $3d^5$ electrons of Fe^{3+}. The optical absorption edge observed at ~450 nm with lower intensity is characteristic of Fe-doped compounds associated with the Fe^{3+}–Fe^{3+} double-excitation process. Coupled with an optical bandgap red shift, electrocatalytic studies of GFO compounds reveal that Fe-doped Ga_2O_3 compound exhibits electrocatalytic activity in contrast to intrinsic Ga_2O_3. Fe-doped samples (GFO) demonstrated appreciable electrocatalytic

activity toward the generation of H_2 through electrocatalytic water splitting, which is attributed to the cumulative effect of different mechanisms such as doping resulting in new catalytic centers, enhanced conductivity, and electron mobility. Hence, the electrocatalytic behavior of Fe-doped Ga_2O_3 resulted due to Fe chemical states and red shift in the optical bandgap.

b-Crystalline phase gallium oxide (*b*-Ga_2O_3) is an ultrawide bandgap material with prospective applications in electronics and deep ultraviolet (DUV) optoelectronics and optics. The monoclinic crystal structure of *b*-Ga_2O_3 results in optical anisotropy to incident light with different polarization states. This attribute can lead to different optical applications in the DUV. The optical properties of *b*-Ga_2O_3 thin films grown by the pulsed laser deposition technique on sapphire substrates with different crystallographic orientations were reported in [30]. Marked in-plane polarization anisotropy, determined by reflectance and Raman spectroscopy, was observed for *b*-Ga_2O_3 films deposited on an *r*-cut sapphire substrate. In contrast, isotropic optical properties were observed in *b*-Ga_2O_3 films deposited on a *c*-cut sapphire substrate.

Chemical and photochemical processes at semiconductor surfaces are highly influenced by the size of the bandgap, and the ability to control the bandgap by particle size in nanomaterials is part of their promise. The combination of soft x-ray absorption and emission spectroscopies provides bandgap determination in bulk and nanoscale itinerant electron semiconductors such as CdS and ZnO, but this approach has not been established for materials such as iron oxides that possess band-edge electronic structure dominated by electron correlations. Soft X-ray spectroscopy at the oxygen *K*-edge were performed in [31] to reveal the band-edge electronic structure of bulk and nanoscale hematite. Good agreement was found between the hematite bandgap derived from optical spectroscopy and the energy separation of the first inflection points in the X-ray absorption and emission onset regions. By applying this method to two sizes of phase-pure hematite nanoparticles, no evidence for size-driven change in the bandgap of hematite nanoparticles down to around 8 nm was found.

The impact of Ga doping on the properties of α-Fe_2O_3, i.e. α-$Ga_xFe_{2-x}O_3$ (x=0.00, 0.20, 0.40, 0.60) nanospheres synthesized via novel hydrothermal technique was studied, and the structural alterations, dielectric response, and magnetic characteristics were explored. The hexagonal framework containing a rhombohedral lattice arrangement of α-$Ga_xFe_{2-x}O_3$ (x=0.00, 0.20, 0.40, and 0.60) nanoparticles was confirmed by rigorous analysis using X-ray diffraction (XRD) and Rietveld refinements. Nanospheres with impressive mono dispersity and an average diameter of 63 nm were determined by scanning electron microscopy. Magnetic investigations revealed diluted antiferromagnetic spin order within Ga-doped α-Fe_2O_3 nanoparticles marking a significant increase in the coercivity from 1595.28–2343.46 Oe (x=0.00–0.60). The observable remnant magnetization patterns illustrated the significance of Ga^{3+} doping in enhancing the magnetic characteristics of α-Fe_2O_3 attributed to the presence of uncompensated spin values between neighboring rhombohedral layers where opposite spin orientations coexist. A detailed dielectric analysis of α-$Ga_xFe_{2-x}O_3$ (x=0.00, 0.20, 0.40, and 0.60) nanoparticles was conducted to determine the dielectric constant (ε), dielectric loss (tanδ), ac-conductivity, complex impedance components, and the hopping probability of electron fluctuation with frequency. In

the cole-cole plot for α-$Ga_xFe_{2-x}O_3$ (x=0.20, 0.40, and 0.60), the dominating grain boundary effect in conduction was indicated.

New luminescence aspects about gallium oxide powders by intra-bandgap photoluminescence (PL) measurements were performed in [32]. In contrast to the generally accepted results of the earlier works done by many researchers, the nitrogen impurity was found to obviously play an important role in the luminescence properties of gallium oxides. It was observed that the nitrogen-induced luminescence center leads to the new UV emission band around 3.47 eV with narrow linewidth from both a- and b-Ga_2O_3. This demonstrated that a- and b-Ga_2O_3, despite the different crystal structure, have the same nitrogen-induced luminescence mechanism. It was also found that the nitrogen in gallium oxides acts as a shallow donor whose ionization energy is 12–15 meV.

The influence of growth time on the structural, optical, and optoelectronic properties of b-Ga_2O_3 films produced on Si substrates by the chemical vapor deposition method was studied in [33]. The prepared films were characterized by XRD, field-emission scanning electron microscopy, and UV–Vis spectrophotometry. The films exhibited a mixed phase (β-α)-Ga_2O_3 crystal structure with crystallite size ranging between 34.98 and 164.69 nm and bandgap increased from 4.74 to 4.88 eV. The absorption and extinction coefficients were in the order of 10^3 and 10^{-1}, respectively. The refractive index, dispersive energy and single oscillator energy increased from 1.86 to 1.87, 19.24 to 28.64, and 8.36 to 9.54, respectively, with the increase in growth time. The oscillator strength, oscillator wavelength, third-order nonlinear optical susceptibility and dispersion of refractive index were in the order of 10^{-4}, 10^{-2}, 10^{-10} and 10^{-9}, respectively. The carrier concentration, optical conductivity, optical mobility, and optical resistivity were also evaluated. The real and imaginary dielectric constants, and plasmon frequency were also determined.

Enhanced red shift in the optical bandgap of b-Ga_2O_3 films was reported in [34]. Intrinsic and N-incorporated b-Ga_2O_3 nanostructures were deposited on Si substrates by the hydrogen reducing-ambient chemical vapor deposition method. The effects of N addition on the structural, morphological, optical and photoelectrochemical properties were studied appropriately. XRD analysis showed decreasing crystallite size from 165.2 to 38.2 nm with increasing NH_3 flow rate. Microstructural observations by field-emission scanning electron microscopy exhibited morphology transformation from nanobelts to full nanoclumps. Energy dispersive X-ray analysis revealed N concentration from 0 up to 17.1 at.% with rising ammonia flow rate. Optical reflectance measurements by UV–vis–NIR spectrophotometry showed enhanced narrowing of optical bandgap from 4.87 to 3.54 eV attributed to rising N content. Photoelectrochemical performance of the doped b-Ga_2O_3 films, measured in 0.1 M HCl electrolyte showed significant photo-response with photocurrent density up to 0.347 mA/cm^2 and 0.1% photon-to-current conversion efficiency.

CONCLUSION

Optical diffuse reflectance spectroscopy (ODRS) measurements were performed on gallium oxide-hematite equimolar mixture over the entire UV-VIS-NIR range. There was no optical

absorbance below the bandgap of hematite determined using Tauc plots, for none of the ball milling times. Above the bandgap, the optical absorbance was enhanced and broadened, depending on the milling time employed.

Optical absorption bands for hematite and gallium oxide nanopowders were identified. Comparative features in the optical absorption spectra of the nanostructures were discussed (bandgap shift, defect/strain effects, thin film orientation, doping impact and photocatalytical applications). The optical absorption measurements revealed changes in the optical properties of the gallium oxide-hematite nanoparticles system as a function of milling processing parameters.

ACKNOWLEDGMENT

This work was supported in part by the National Science Foundation, USA under grants number DMR-0854794 and DMR-1002627-1. J.A. and J.K. acknowledge the support of the National Science Foundation, USA under grant DMR-1611198.

Conflicts of Interest

There are no conflicts of interest regarding the work described in this paper.

References

[1]. Rozenberg, G., et al., *High pressure structural studies of hematite*. Physical Review B, 2002. 65: p. 064112.

[2]. Bergenmayer, W., et al., *Ab Initio thermodynamics of oxide surfaces: Oxygen on hematite (0001)*. Physical Review B, 2004. 69: p. 195409.

[3]. Zheng, Y., et al., *Quasicubic hematite nanopartcles with excellent catalytic performance*. Journal of Physical Chemistry, 2006. 110: p. 3093-3097.

[4]. Wu, C., et al., *Synthesis of hematite nanorods: Diameter-size and shape effects on their applications in magnetism, lithium ion battery, and gas sensors*. Journal of Physical Chemistry, 2006. 110: p. 17806-17812.

[5]. Liu, J.Z., *Morin transition in hematite doped with Iridium ions*. Journal of Magnetism and Magnetic Materials, 1986. 54-57: p. 901-902.

[6]. Stroh, C., et al., *Ruthenium oxide-hematite magnetic ceramic nanostructures*. Ceramics International, 2015. 41: p. 14367-14375.

[7]. Jewel, M.U., et al., *A comprehensive study of defects in gallium oxide by density functional theory.* Computational Materials Science, 2023. 218: p. 111950.

[8]. Zhang, D., et al., *Ambient-condition strategy for rapid mass production of crystalline gallium oxide nanoarchitectures toward device application*. Journal of Materials Science & Technology, 2023. 163: p. 150-157.

[9]. Chen, Y., et al., *Bandgap engineering of gallium oxides by crystalline disorder*. Materials Today Physics, 2021. 18: p. 100369.

[10]. Zhang, J., et al., *Deep UV transparent conductive oxide thin films realized through degenerately doped wide-bandgap gallium oxide*. Cell Reports Physical Science, 2022. 3: p. 100801.

[11]. Lorenzi, R., et al., *Defect-assisted photocatalytic activity of glass-embedded gallium oxide nanocrystals.* Journal of Colloid and Interface Science, 2022. 608: p. 2830-2838.

[12]. Chen, Y., et al., *Electronic States of gallium oxide epitaxial thin films and related atomic arrangement*. Applied Surface Science, 2022. 578: p. 151943.

[13]. Ramana C.V., et al., *Electronic structure and chemical bonding in transition-metal-mixed gallium oxide compounds.* Journal of Physics and Chemistry of Solids, 2021. 157: p. 110174.

[14]. Sudrajat, H., et al., *Gallium oxide nanoparticles prepared through solid-state route for efficient photocatalytic overall water splitting*. Optik, 2020: p. 165370.

[15]. Su, T., et al., *High-rate growth of gallium oxide films by plasma-enhanced thermal oxidation for solar-blind photodetectors*. Applied Surface Science, 2023: p. 157162.

[16]. Falkova, A.N., et al., *Mechanoactivated interaction of hematite and gallium*. Journal of Alloys and Compounds, 2009: p. 31-34.

[17]. Manandhar, S., et al., *Optical constants of titanium-doped gallium oxide thin films*. Optical Materials, 2019: p. 109223.

[18]. Almaev, A.V., et al., *Oxygen sensors based on gallium oxide thin films with addition of chromium.* Superlattices and Microstructures, 2020: p. 106392.

[19]. Jubu, P.R., et al., *Synthesis and characterization of gallium oxide in strong reducing growth ambient chemical vapor deposition*. Materials Science in Semiconductor Processing, 2021: p. 105361.

[20]. Mallesham, B., et al., *Crystal chemistry, band-gap red shift, and electrocatalytic activity of iron-doped gallium oxide ceramics.* ACS OMEGA, 2020: p. 104-112.

[21]. Ho, Y.C., et al*., Deep ultraviolet optical anisotropy of gallium oxide thin films*. ACS OMEGA, 2024: p. 27963-27968.

[22]. Singh, A., et al., *Intra- and inter-conduction band optical absorption processes in gallium oxide*. Applied Physics Letters, 2020: p. 072103.

[23]. Gilbert, B., et al., *Band-gap measurements of bulk and nanoscale hematite by soft-ray spectroscopy*. Physical Review B, 2009: p. 035108.

[24]. Krehula S., et al*., Synthesis and microstructural properties of mixed iron-gallium oxides*. Journal of Alloys and Compounds, 2015: p. 130-141.

[25]. Irshad, I., et al., *Tuning of magnetic and dielectric properties of gallium doped hematite nanospheres*. Journal of Alloys and Compounds, 2024: p. 173901.

[26]. Cho, S., et al., *New luminescent band due to nitrogen impurities in gallium oxide powders*. Materials Letters, 2012: p. 1004-1009.

[27]. Jubu, P.R., et al., *Optical and optoelectronic properties of gallium oxide films fabricated by the chemical vapor deposition method*. Physica B: Condensed Matter, 2024: p. 415763.

[28]. Jubu, P.R., et al., *Enhanced red shift in optical absorption edge and photoelectrochemical performance of N-incorporated gallium oxide nanostructures*. Vacuum, 2020: p. 109704.

[29]. Glasser, S., et al., *Effects of mechanochemical activation on the structural, magnetic and optical properties of yttrium iron garnet-graphene nanoparticles*. Physica B, 2023. 650: p. 414501.

[30]. Sorescu, M., et al., *Formation of skyrmion phase in the Fe-Co-Si system by mechanochemical activation*. Physica B, 2024. 688: p. 416153.

[31]. Glasser, S., et al., *Synthesis and characterization of gadolinium oxide-hematite magnetic ceramic nanostructures.* Journal of Minerals and Materials Characterization and Engineering, 2023. 11: p. 1-15.

[32]. Sorescu, M., et al., *Mechanochemical synthesis and Mössbauer characterization of neodymium oxide-hematite magnetic ceramic nanoparticles: Phase sequence and recoilless fraction*. Materials Chemistry and Physics, 2022. 277: p. 125511.

[33]. Diamandescu, L. et al., *Multifunctional $GaFeO_3$ obtained via mechanochemical activation followed by calcination of equimolar nanosystem gallium oxide-hematite.* Nanomaterials, 2021. 11: p.57.

[34]. Diaz-Guerra, C., et al., *Magnetic transitions in hematite nanowires*. Journal of Applied Physics, 2009. 106: p. 104302.